POLITECNICO DI TORINO
Repository ISTITUZIONALE

Final nanoparticle size distribution under unusual parameter regimes

(Article begins on next page)

18 July 2024

Final nanoparticle size distribution under unusual parameter regimes

Elena Sabbioni,[1] Rebeka Szabó,[2] Paola Siri,[1] Daniele Cappelletti,[1] Gábor Lente,[2] and Enrico Bibbona[1]

[1)]*Department of Mathematical Sciences, Politecnico di Torino, Torino, Italy*

[2)]*Department of Physical Chemistry and Materials Science, University of Pécs, Pécs, Hungary*

(*Electronic mail: elena.sabbioni@polito.it, rebekasz@gamma.ttk.pte.hu)

(Dated: 7 June 2024)

We explore the large-scale behavior of a stochastic model for nanoparticle growth in an unusual parameter regime. This model encompasses two types of reactions: nucleation, where *n* monomers aggregate to form a nanoparticle, and growth, where a nanoparticle increases its size by consuming a monomer. Reverse reactions are disregarded. We delve into a previously unexplored parameter regime. Specifically, we consider a scenario where the growth rate of the first newly formed particle is of the same order of magnitude as the nucleation rate, in contrast to the classical scenario where in the initial stage nucleation dominates over growth.

In this regime, we investigate the final size distribution as the initial number of monomers tends to infinity through extensive simulation studies utilizing state-of-the-art stochastic simulation methods with an efficient implementation and supported by high-performance computing infrastructure. We observe the emergence of a deterministic limit for the particle's final size density.

To scale up the initial number of monomers to approximate the magnitudes encountered in real experiments, we introduce a novel approximation process aimed at faster simulation. Remarkably, this approximating process yields a final size distribution that becomes very close to that of the original process when the available monomers approach infinity. Simulations of the approximating process further support the conjecture of the emergence of a deterministic limit.

I. INTRODUCTION

Nanoparticles, ranging in size from 1 to 1000 nanometers, hold immense potential in various fields, including catalysis[1], electronics[2], medicine[3], and environmental remediation[4]. Their unique properties, stemming from their small size and large surface area-to-volume ratio, make them particularly intriguing. Understanding the kinetics of nanoparticle formation and managing their size distribution are essential steps to ensure optimal functionality and minimize potential toxicity[5] across diverse applications.

The process of nanoparticle formation shares similarities with established polymerization processes. It can be explained by various models. The foundational framework for this kind of process is the Smoluchowski model. It explains the stochastic motion of particles in a fluid, known as Brownian motion, and provides a mathematical explanation for particle aggregation. In some cases for the reversible case[6,7], as well, which can be interpreted by both stochastically and deterministically. The LaMer model offers a detailed explanation of the kinetics involved[8,9] in nanoparticle formation. According to this model, nanoparticle formation occurs through instantaneous nucleation, followed by a series of growth steps facilitated by the addition of monomers.

The size distribution of isothermal crystallization processes through nucleation and growth can also be described by the Johnson-Mehl-Avrami-Kolmogorov model, in which the rates of the two reactions cannot change, the nuclei begin to grow at the same time[10–12]. It is also important to mention the Finke-Watzky model[13,14], which introduces the concept of a slow nucleation reaction followed by a rapid autocatalytic growth step. This model has undergone further developments employing mechanism-enabled population balance equations[15,16]. Beyond these classical models, there are several other approaches in the literature, most of them take into account the thermodynamic properties, as well, which are not spelled out here.

The Becker-Döring model is a mathematical model of aggregation and fragmentation that is based on very similar steps. Its most common formulation is in terms of an infinite system of ordinary differential equations[17–19]. By employing a coarsening step, the discrete space of the particle sizes can be mapped to a continuous limit domain, and consequently the deterministic Becker-Döring model converges to a transport partial differential equation named after Lifshitz-Slyozov[20,21].

Stochastic models are often considered more realistic, at least at small scales, since they can track the random events of individual monomer attachments or detachments. A stochastic analog of

2

the Becker-Döring model has been investigated[22] and it has been shown that, at a large scale and with suitably balanced reaction rates, it converges to the deterministic Becker-Döring limit. This approach is based on a so-called *classical scaling* where in the first place only nucleation occurs, and only after a large portion of the monomers has been spent in nucleations, the growths start to take place. As a result, many particles are created with a distribution of the particle sizes (measured in monomer units) that remains concentrated around low counts.

The convergence to a deterministic limit bears significant practical implications, implying that even inherently stochastic phenomena can manifest as deterministic when observed at appropriate scales. This facilitates investigation via a single experimental realization, obviating the need for multiple repetitions.

In this paper, we introduce a stochastic Markov model of nanoparticle formation, once again relying on nucleation and growth. Its convergence to a deterministic limit is well understood in the so-called classical scaling, due to its strong similarity to the stochastic Becker-Döring model[22]. Some of the latest results have derived some general explicit and approximated solutions for the final average sizes of its deterministic limit[23–26].

In real experiments of nanoparticles growth[27–29], the final size of the particles can have a wide range (typically from 1 to 100 nm, but up to 1000 is possible). Small nanoparticles (a few tens of nanometers) are reasonably described by our model under the classical scaling. However, large particles[30] with diameters of $10^2 - 10^3$ nm, may incorporate a huge number of monomers. This regime is hardly explainable under the classical scaling and the existence of a deterministic limit size distribution is not guaranteed by the classical theory.

Assuming a novel scaling of the rate constants that has never been addressed before, such that growths and nucleations are in a balanced competition from the ealiest moments, we provide computational evidence that a deterministic limit size distribution still emerges. Moreover, this distribution is compatible with the formation of the large nanoparticles mentioned above. In particular, we investigate the model predictions through a simulation study that uses the most advanced methods[31,32] with an efficient implementation in the Julia programming language[33] run on a high-performance computing infrastructure.

Since the computational cost for this complex model remains a substantial limitation, the size of the system cannot be raised to the order of magnitudes that would be realistic in any experimental setting. To overcome this limitation, we develop an approximated model that can be simulated

3

much faster and that appears to keep the same final size distribution when size of the system grows very big. Utilizing this novel approximating process, we achieved notable enhancement in the quantity of monomer units accessible, nearing levels anticipated in actual experimental scenarios[27–29], and further strengthens the computational evidence of convergence towards a deterministic limit.
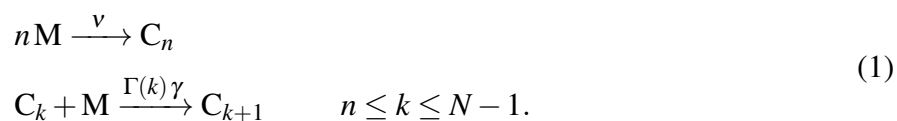
A mathematical proof of the conjectured convergence and a tractable expression for the final size distibution would be highly desirable, but are not adressed in this paper. We hope that our contribution will stimulate further advancements in this direction.

II. THEORY AND COMPUTATIONAL DETAILS

A. The model

We model nanoparticle formation as a process comprising an nth-order nucleation step and second-order irreversible growth steps. In the initial stage, a group of n monomer units comes together to form a kinetically effective nucleus, which then continues to grow as one monomer unit at a time is added to a single nanoparticle.

We define a stochastic model whose state is given by $(x_0, x_1, \ldots, x_N)$ where x_0 refers the monomer unit counts, while $x_i, i \geq 1$ gives the counts of nanoparticles of size i. All of them evolve according to the occurrence of the following reactions

$$
\begin{aligned}
n\text{M} &\xrightarrow{\nu} \text{C}_n \\
\text{C}_k + \text{M} &\xrightarrow{\Gamma(k)\gamma} \text{C}_{k+1} \qquad n \leq k \leq N-1.
\end{aligned}
\tag{1}
$$

In the above equations, M denotes a monomer unit, while C_k represents a nanoparticle containing exactly k monomer units in it, which we define as a particle of size k. Throughout the paper particle sizes are always measured in monomer units, not directly in nanometers. The initial number of monomer units is N. The stoichiometric vectors $\mathbf{v}_k$, where $k = 0, 1, \ldots, N-1$, are $N+1$-dimensional vectors with

$$
\mathbf{v}_k = \begin{cases}
-n\mathbf{e}_1 + \mathbf{e}_{n+1} & k = 0 \\
\mathbf{0}_{N+1} & 1 \leq k \leq n-1 \\
-\mathbf{e}_1 - \mathbf{e}_{k+1} + \mathbf{e}_{k+2} & n \leq k \leq N-1
\end{cases}
$$

4

where $\mathbf{0}_{N+1} \in \mathbb{R}^{N+1}$ is the null vector, while $\mathbf{e}_k \in \mathbb{R}^{N+1}$ is a vector with the k-th component equal to 1 and all other components equal to 0, and the stoichiometric matrix $S \in \mathbb{R}^{(N+1) \times N}$ is

$$
\mathbf{S} = \begin{bmatrix} \mathbf{v}_0 & \mathbf{v}_1 & \dots & \mathbf{v}_{N-1} \end{bmatrix} = \begin{bmatrix}
-n & 0 & \cdots & 0 & -1 & -1 & -1 & \cdots & -1 & -1 \\
0 & 0 & \cdots & 0 & 0 & 0 & 0 & \cdots & 0 & 0 \\
\vdots & \vdots & \vdots & \vdots & \vdots & \vdots & \vdots & \vdots & \vdots & \vdots \\
0 & 0 & \cdots & 0 & 0 & 0 & 0 & \cdots & 0 & 0 \\
+1 & 0 & \cdots & 0 & -1 & 0 & 0 & \cdots & 0 & 0 \\
0 & 0 & \cdots & 0 & +1 & -1 & 0 & \cdots & 0 & 0 \\
0 & 0 & \cdots & 0 & 0 & +1 & -1 & \cdots & 0 & 0 \\
\vdots & \vdots & \vdots & \vdots & \vdots & \vdots & \vdots & \vdots & \vdots & \vdots \\
0 & 0 & \cdots & 0 & 0 & 0 & 0 & \cdots & +1 & -1 \\
0 & 0 & \cdots & 0 & 0 & 0 & 0 & \cdots & 0 & +1
\end{bmatrix}. \tag{2}
$$

The dynamics proceeds according to a continuous-time Markov Chain $\mathbf{X}(t) = (X_0(t), X_1(t), \ldots, X_N(t))$, with reaction rates

$$
\lambda_0(x_0, x_1, \ldots, x_N) = \nu \frac{x_0!}{(x_0 - n)!} \tag{3}
$$

$$
\lambda_k(x_0, x_1, \ldots, x_N) = 0 \qquad\qquad 0 < k < n
$$

$$
\lambda_k(x_0, x_1, \ldots, x_N) = \gamma \Gamma(k) x_0 x_k \qquad\qquad n \leq k \leq N-1 \tag{4}
$$

with $\lambda_0(x_0, x_1, \ldots, x_N)$ in (3) being the nucleation rate and $\lambda_k(x_0, x_1, \ldots, x_N)$ the rate at which nanoparticles of size k are grown into particles of size $k+1$. The Markov model characterized above allows for the following representation

$$
\mathbf{X}(t) = \mathbf{X}(0) + \sum_{k=0}^{N-1} \mathbf{v}_k Y_k \left(\int_0^t \lambda_k(\mathbf{X}(s)) ds \right) \tag{5}
$$

in terms of the independent unit rate Poisson processes Y_k[34].

In the literature, different expressions for the function $\Gamma(k)$ have been proposed. The most popular choices are four. The *mass kernel* operates under the assumption that a nanoparticle's reactivity is directly proportional to its mass, which is described by the function $\Gamma(k) = k$. The *surface kernel* considers the reactivity of a nanoparticle as being proportional to its surface area, $\Gamma(k) = k^{2/3}$. The *Brownian kernel*, based on the reactivity of a nanoparticle being proportional to

5

its radius, $\Gamma(k) = k^{1/3}$. The *diffusion kernel* assumes that a nanoparticle's reactivity is independent of its size which mirrors the size independence of the diffusion-controlled rate constant, where their larger reactive cross-section offsets the lower mobility of larger particles. This constant function is denoted by $\Gamma(k) = 1$, implying that all the particles grow at the same rate, regardless of their dimension. In the context of this paper, we focus on the diffusion kernel alone.

Monomers are utilized in both the nucleation and growth processes, resulting in a continuous decrease in the number of monomer units over time until it reaches zero. Once this point is reached, no further reactions can occur, indicating that each particle created has attained its final size. Consequently, the final size distribution emerges as a significant characteristic of the model and is inherently random: distinct instances of the process yield varying final size distributions. Computing the probability law of this final size distribution is exceedingly complex, and simulations are the only feasible approach.

1. *Deterministic limits under the classical scaling*

The size distribution of the stochastic model described above is known to approach a deterministic limit under a suitable scaling of the rate constants, known as *classical scaling*. This convergence result is achieved by combining two classical findings. First, under the classical scaling, the stochastic model converges to an infinite set of ordinary differential equations (ODEs) known as the Becker and Döring equations[22,35], which describe the concentrations of particles of any given size. Second, the ODE system itself, once the particle sizes are binned and rescaled to a continuum, converges to a deterministic distribution that satisfies a partial differential equation (PDE) model known as the Lifshitz–Slyozov model[20,36,37].

We do not intend to delve into a detailed mathematical exposition of the known theory here. Rather, we aim to highlight that if the rate constants and initial conditions scale as

$$\mathbf{X}(0) \sim N, \qquad \nu \sim \frac{1}{N^{n-1}}, \qquad \gamma \sim \frac{1}{N}, \tag{6}$$

when $N \to \infty$, a deterministic limit size distribution is known to emerge, after rescaling the sizes to the continuum. Under this so-called *classical scaling*, if we start with a monomer population of size N, initially the nucleation rate (3) dominates the growth rates (4) until most of the monomers are spent. However, the available monomers steadily decrease and so does the nucleation rate, up to when the growth reactions will enter the competition allowing for the created

6

particles to increase their size. Under such a scaling we expect to find a *large* number of particles (order N) while the typical size is *small* (order 1). As mentioned in the Introduction, parameters regimes corresponding to the the classical scaling seem to be compatible with the formation of small nanoparticles with a size of a few tens of nanometers. Indeed, given that the diameter of a monomer is of the order of 10^{-1} nm, such a *small* nanoparticle would consist of approximately a hundred monomers along its diameter, resulting in a total of about 10^6 monomers incorporated in its volume. Consequently, the number of monomers in such a particle would be negligible compared to the initial number of available monomers, which could be around $N = 10^{24}$.

2. An alternative scaling

As detailed in Section II A 1, the limiting behavior of the chemical reaction network (1) is well-understood under the classical scaling. However, other regimes may also be of interest. In particular, we explore the evolution of the nanoparticles' final size when the initial conditions and reaction rate constants scale as

$$X(0) \sim N, \qquad \nu \sim \frac{1}{N^{n-1}}, \qquad \gamma \sim 1.$$

Under this condition, whenever the first particle is created, its growth rate (4) and the nucleation rate (3) are both of order N. The competition between nucleation and growth starts earlier compared to the classical scaling, and we expect to create less particles, that are grown to a larger size. The largest diameter for a nanoparticle is of order 10^3 nm, which implies approximately 10^4 monomers along the diameter and 10^{12} in total. We aim to determine whether this scaling can explain the formation of these large particles. Additionally, we address the specific question of whether, under this regime, a deterministic limit for the final size distribution can still emerge. To this end, we establish a simulation study outlined in Section II B.

B. Simulations

The investigation of large size stochastic models is most often unfeasible with probabilistic techniques alone, making the use of numerical simulations unavoidable. Moreover, when the size of the system gets very large even exact simulation methods are unable to cope with the complexity of the system because of too long running time or of too heavy memory requirements.

7

We quickly review in this section the state of the art methods (both exact and approximate) that may be employed to simulate our model. We present them in a form that is tailored to our system and tries to spare unnecessary resources.

1. Gillespie's algorithm

Gillespie's algorithm (or Stochastic Simulation Algorithm (SSA)) operates by simulating each event of a continuous-time Markov chain that tracks the evolution of the process[31,38,39]. Consider t as the current time and $X(t)$ as the present state of the system. Let $t + \tau$ and r be respectively the time at which the next reaction occurs and the index of the reaction firing at $t + \tau$. The algorithm generates τ from an exponential distribution with mean equal to the sum of all reaction rates $\sum_{k=0}^{N-1} \lambda_k$, while the index r is then simulated as a random variable with values $0, 1, \cdots, N-1$ and associated probabilities $\frac{\lambda_0(X(t))}{\sum_{k=0}^{N-1} \lambda_k(X(t))}, \frac{\lambda_1(X(t))}{\sum_{k=0}^{N-1} \lambda_k(X(t))}, \cdots, \frac{\lambda_{N-1}(X(t))}{\sum_{k=0}^{N-1} \lambda_k(X(t))}$. Consequently, the system's state is updated as $X(t + \tau) = X(t) + \mathbf{v}_r$. Notably, if L represents the dimension of the largest nanoparticle created up to time t, our chemical reaction network structure ensures $X_k(t) = 0$ and $\lambda_k(X(t)) = 0$ for each $k \geq L + 1$. Given that the primary focus of this work is the final size distribution of the nanoparticles, we are solely interested in determining the next reaction to fire, disregarding the temporal moment in which it fires. From a computational point of view, this allows us to bypass the generation of τ, thereby accelerating the execution. For the same reason, since the first reaction is for sure a nucleation, we can directly start to simulate with $N - n$ monomers and 1 particle of size n. Algorithm 1 in the Appendix outlines the pseudo-code of Gillespie's algorithm tailored to our chemical reaction network.

2. Tau-leaping with post-leap checks

The tau-leaping method[40] in many cases provides a significant computational speedup compared to exact algorithms, while maintaining a high-quality approximation. However, in the context of our model, a challenge arises with the original tau-leap method[41], as it can lead to physically unrealistic negative populations due to the unboundedness of the Poisson random variable. To address this concern, we adopt an adaptive version of the tau-leap algorithm proposed by Anderson[32]. This adaptive approach incorporates post-leap checks at each step, thereby preventing the exploration of infeasible states.

Let t denote the absolute time of the system. Assume we know the current state $X(t) = (X_0(t), X_1(t), \ldots, X_N(t))$ and the propensities vector $\lambda = (\lambda_0(X(t)), \ldots, \lambda_N(X(t)))$. Here, $\lambda_0(X(t))$ denotes the rate function associated with the nucleation and $\lambda_k(X(t))$, with $1 \leq k \leq N-1$, is related with the growth of a nanoparticle from dimension k to dimension $k+1$. To simplify the notation in the following discussion, we drop the explicit dependence of the propensity scores on the state, denoting them as λ_k. Additionally, let Y_k, with $k = 0, \ldots, N-1$, be a unit rate Poisson process related to the k-th reaction. Suppose we are aware of the internal time of each process, $T_k(t) := \int_0^t \lambda_k(X(s)) ds$, and of its number of firings up to time t, $C_k(t) := Y_k(T_k(t))$. As in Gillespie's algorithm described in Section II B 1, let L denote the dimension of the largest nanoparticle created up to time t. Once more, leveraging the structure of the chemical reaction network, for each $k \geq L+1$, we have $\lambda_k = 0$, $T_k(t) = 0$, and $C_k(t) = 0$. This observation yields a significant acceleration in computational time by avoiding the computation of unnecessary quantities, as highlighted in Algorithm 2.

After adaptively determining τ, the algorithm[32] proposes a new leap with τ and we are interested in the value of the Poisson processes $\{Y_k\}_{k=0,\ldots,N-1}$ when the internal times are $\{T_k(t) + \lambda_k \tau\}_{k=0,\ldots,N-1}$. If we lack information about the state of the Poisson processes in the future, i.e. we do not know $Y_k(T)$ for $T > T_k(t)$, the number of possible jumps of Y_k in $[T_k, T_k + \lambda_k \tau]$ follows a Poisson distribution with rate $\lambda_k \tau$. Consequently the algorithm generates the corresponding N independent Poisson random variables, $J_0, \ldots, J_{N-1}$, and set $Y_k(T_k(t) + \lambda_k \tau) = C_k(t) + J_k$, for $k = 0, \ldots, N-1$. At this point, we must verify if all reactions satisfy the leap condition, i.e.

$$
|\mathbf{S} \cdot \mathbf{J}| \leq \begin{bmatrix} \max\left(\varepsilon X_0(t)/g_0, 1\right) \\ \max\left(\varepsilon X_1(t)/g_1, 1\right) \\ \vdots \\ \max\left(\varepsilon X_N(t)/g_N, 1\right) \end{bmatrix} \tag{7}
$$

where $\mathbf{S}$ is the stoichiometric matrix (2), $\mathbf{J} = [J_0 \ J_1 \ \cdots \ J_{N-1}]^t$ and $g_i := g_i(X_i(t))$ is a prescribed function described by Anderson[32]. Note that the inequality in equation (7) is interpreted component-wise, and the leap condition is deemed satisfied if the inequality is verified for each component. In our scenario, $g_i(X_i(t)) = 2$ for each $i \geq 1$, whereas the value of g_0 relies on the

9

number *n* of monomers consumed during nucleation. Specifically,

$$g_0(X_0(t)) = \begin{cases} 1 & \text{if } n = 1 \\ 2 + \frac{1}{X_0(t)-1} & \text{if } n = 2 \\ 3 + \frac{1}{X_0(t)-1} + \frac{2}{X_0(t)-2} & \text{if } n = 3 \end{cases}$$

For our system (1), the leap condition presented in equation (7) translates to

$$\begin{cases} \left| -nJ_0 - \sum_{k=1}^{L} J_k \right| \leq \max\left(\varepsilon X_0(t)/g_0, 1\right) \\ \left| -J_n + J_0 \right| \leq \max\left(\varepsilon X_n(t)/2, 1\right) \\ \left| -J_i + J_{i-1} \right| \leq \max\left(\varepsilon X_i(t)/2, 1\right) & \text{for } i = n+1, \dots, L \\ \left| J_L \right| \leq \max\left(\varepsilon X_{L+1}(t)/2, 1\right) \end{cases} \tag{8}$$

If condition (7) is satisfied, the leap is accepted, we update the state of the system as

$$\mathbf{X}(t+\tau) = \mathbf{X}(t) + \mathbf{S} \cdot \mathbf{J}$$

and we attempt the following update. Furthermore, if $J_L > 0$, indicating the creation of a particle with dimension $L + 1$, we increment L by 1 accordingly. On the other hand, if the leap condition fails to hold, the leap is rejected, and we try a new leap with a shorter time step. Specifically, we reduce the time step value, selecting $\tau^* = p\tau$, where $p < 1$. This subsequent attempt must account for the information obtained previously, meaning that we need to consider that $Y_k(T_k(t) + \lambda_k \tau) = C_k(t) + J_k$, to avoid altering the chain's distribution. Theorem 3.1 in the original paper[32] guarantees that the conditional distribution of $Y_k(T_k(t) + \lambda_k \tau^*) - Y_k(T_k(t))$ given that $Y_k(T_k(t)) = c_k$, and $Y_k(T_k(t) + \lambda_k \tau) = c_k + j_k$ is Binomial with number of trials j_k and probability of success $\frac{\tau^*}{\tau}$, for any allowed value for the constants c_k and j_k.

Therefore, the value of the Poisson processes in $T_k(t) + \lambda_k \tau^*$ are now simulated according to a binomial distribution and the leap condition (7) is checked for the new leap. If the condition is not met, the information we have just obtained is retained and employed to compute the value of the Poisson processes with a shorter time step. Conversely, if the condition is satisfied, we accept the update and adjust the state of the system accordingly.

It's crucial to emphasize that when we reject a leap, we are solely storing information regarding the future values of the Poisson processes $Y_k(T_k + \lambda_k \tau)$, rather than the values of our chain $\mathbf{X}(t+\tau)$. Moreover, we may reject multiple leaps, leading to the storage of numerous different values of

10

$Y_k(T)$. When we attempt a new leap at time $\tilde{T}$, the newly proposed internal time may exceed the last stored internal time, or it may fall between two stored internal times. In the former case, the new value of Y_k is derived from a Poisson random variable, while in the latter scenario, we exploit the binomial distribution. This last distribution just relies on the value of Y_k evaluated at the largest internal time smaller than the newly proposed time. Consequently, after a leap is accepted, all previous values of Y_k can be discarded and will no longer influence the distribution of subsequent leaps. Regarding the value of τ, it is updated not only when a leap is rejected, but also when it is accepted, aiming to adapt the step size according to the behaviour of the system. In particular

- if a leap is rejected, then we decrease τ, setting $\tau = \tau p$, for some $p < 1$;

- if a leap satisfies the leap condition (7) for ε (and therefore it is accepted), but it fails the leap condition with $\frac{3}{4}\varepsilon$, then we decrease τ, setting it equal to τp^*, for some p^* such that $p < p^* < 1$;

- if a leap satisfies the leap condition (7) both with ε and $\frac{3}{4}\varepsilon$, we increase τ, setting $\tau = \tau^q$, for some $0 < q < 1$.

A pseudocode for this algorithm is presented in the Appendix.

III.   RESULTS AND DISCUSSIONS

The existence of a deterministic limit under the alternative scaling (6) is investigated in several numerical examples that use both exact and approximated simulation methods.

A.   Exact simulation results

For $N = 10^4, 10^5, 10^6, 10^7$, and 10^8, we simulate 6 trajectories of the process (5) with parameters given by

$$n = 3, \qquad X(0) = Ne_1, \qquad \gamma = 5, \qquad v = 5 \cdot N^{1-n}$$

Simulations are run until all monomers are consumed and we investigate the final size distribution. We use the Gillespie algorithm introduced in Algorithm 1. The Julia code with our implementation is available at `https://github.com/elenasabbioni/nanoparticles`.

11

Three noteworthy patterns arise from the simulation outcomes, presented in Figure 1.

First, in all simulations, the final size of the nanoparticles is of order $\sqrt{N}$. Therefore, when the sizes are adjusted by scaling them with $\sqrt{N}$, the resulting distributions span the same range, regardless of the value of N or of the specific realization.

Moreover, regardless of the value of N, the counts of particles with any given final size are consistently small, typically amounting to only a few units. Indeed, the typical final size is approximately $\sqrt{N}$, while the number of available monomers is N. Consequently, the typical number of particles formed before exhausting the monomers is also on the order of $\sqrt{N}$. These particles tend to distribute across the entire range of available sizes, with a modest concentration in the most probable region, which is found to be between 1.2 and 1.6 in units of $\sqrt{N}$.

Thirdly, we observe that for relatively low values of N (e.g., $N = 10^4$), there is a significant variability across different realizations. However, as N increases, the final size distributions become more and more similar to each other, suggesting the existence of a deterministic limiting distribution as N approaches infinity.

To validate this hypothesis, it would be beneficial to increase N even further. However, in our model the number of reactions increases with N, making the computational cost of the Gillespie algorithm non-linear in N, as shown in Table I. Consequently, scaling up N to a higher order is not feasible, even when the code is parallelized and runs on a high performance computing machine.

The just mentioned result that no particle will be grown to a size that is much larger than $\sqrt{N}$, allows us to set up a splitting of such a range of the *effective* particle sizes into bins whose amplitude a is such that both the bin size and the number of bins that will be effectively filled (about $\sqrt{N}/a$)) will tend to infinity, e.g. taking $a = N^{\frac{1}{4}}$). In this way we expect that at least some of the bins will collect a number of particles that increases with N so that for $N \to \infty$ a non-negligible fraction of the created particles will accumulate in it. This process smoothens the distribution of counts and helps averaging out the difference between the repetitions.

Figure 2 shows the effect of the binning with $N = 10^8$. Comparing Figures 1 and 2 we observe an increased similarity between the realizations and a smoother resulting final size density. We are therefore even more confident that the final size density is converging to a continuous deterministic limit.

https://doi.org/10.26434/chemrxiv-2024-wh3jv-v2 ORCID: https://orcid.org/0009-0008-8158-0049 Content not peer-reviewed by ChemRxiv. License: CC BY-NC-ND 4.0
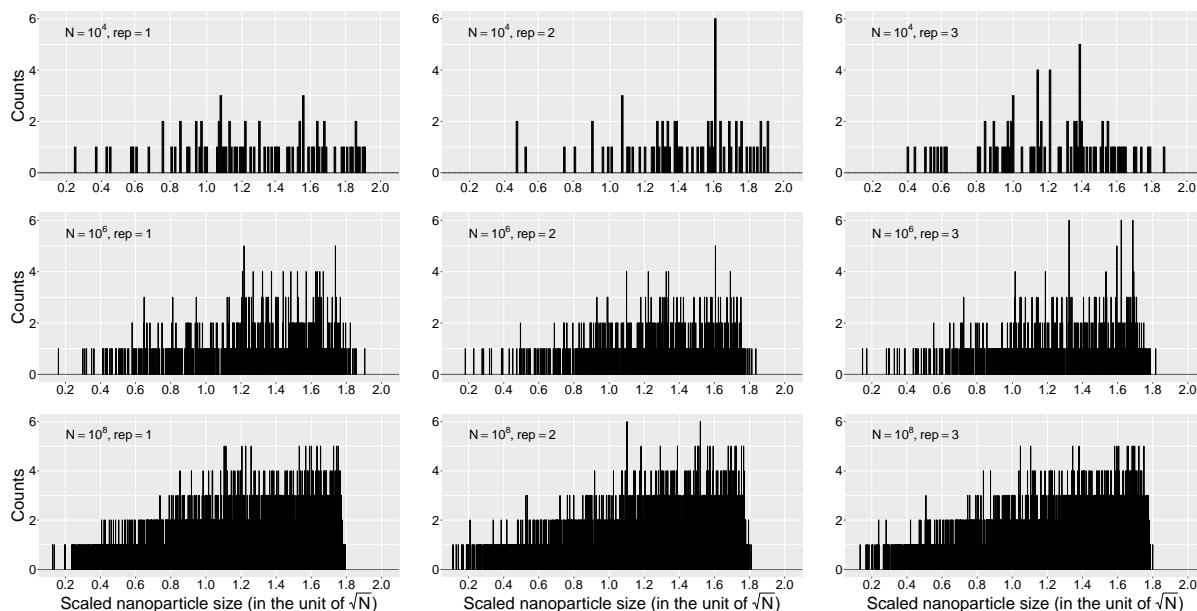
FIG. 1: Final size distribution of the original process (5) with $N = 10^4$ (first row), $N = 10^6$ (second row), $N = 10^8$ (third row). Each column represents a different repetition of the simulation. The results are obtained with the Gillespie's algorithm. The plots present the number of particles for each size, with the x-axis being scaled by $\sqrt{N}$ to ensure that the sizes are independent of N and remain comparable as we increase the initial number of monomers.
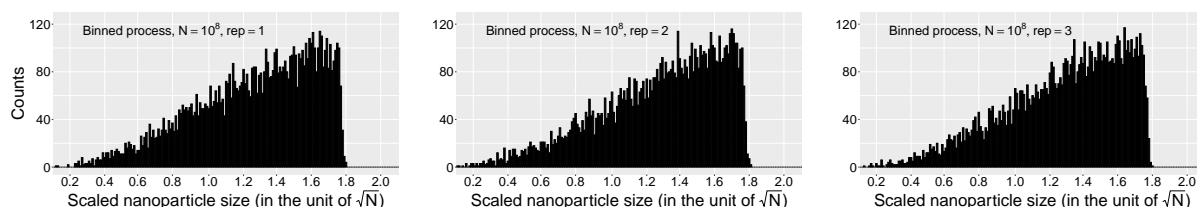

FIG. 2: Final size distribution of the original process (5), after that the state space is binned, with $N = 10^8$. The x-axis is scaled by $\sqrt{N}$.

B. Tau-leap simulation results

Due to the considerable computational expense associated with simulations using the Gillespie algorithm, it is natural to explore a tau-leap approximation, with the hope of being able to simulate the process even when N is of a higher order of magnitude. As previously mentioned in Section III A, the counts of nanoparticles of any given size consistently remain low. Therefore, the basic version of the tau-leap algorithm[41] is inadequate as it often yields negative counts. However, the version of the algorithm that incorporates post-leap checks (cf. Section II B 2) the-

13

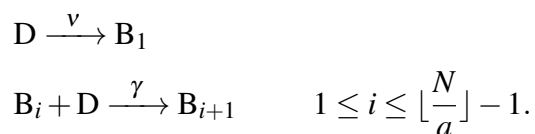| N	Original process		Approximated process	
	Gillespie	Tau-leap	Gillespie	Tau-leap
10^4	1.51	1.98	1.19	1.84
10^6	518.69	225.43	18.52	1.95
10^8	417945.90	192641.70	65.42	2.76
10^{10}	NA	NA	3012.00	13.88
10^{12}	NA	NA	392339.12	194.09
10^{14}	NA	NA	NA	2956.96
10^{15}	NA	NA	NA	14081.16

TABLE I: Time (in seconds) required to simulate $r = 6$ trajectories of both the original process (5) (columns 1 and 2) and the approximated process (columns 3 and 4) in parallel on a cluster with 6 CPUs. The simulations are performed with different initial numbers of monomers N. In instances where the simulation was not feasible, due to an impractical computational time, "NA" values are incorporated into the table.

oretically addresses this issue, and thus, we have implemented the method in this improved form. We begin the simulation study by reproducing the identical settings as previously outlined. This is aimed at facilitating a comparison in both the quality of the approximation and the running time. The quality of the approximation appears to be excellent, as the final size distributions obtained from both methods are practically identical (figures not provided). However, the running times haven't decreased sufficiently to enable scaling by one order of magnitude more. Consequently, the case with $N = 10^9$ still remains beyond reach. The limited speed improvement with the tau-leap method is once more attributed to the prevalence of low counts. Negative numbers continue to be suggested frequently and subsequently discarded due to failures in post-leap checks. This phenomenon results in an additional overhead in each simulation step and a decrease in adaptive step-size to values that are comparable to the waiting time for the next reaction, thereby nullifying the advantage over an exact algorithm.

14

C. An approximating process

As the tau-leap approximation fails to scale to higher orders of magnitude in N, we introduce a new process designed for faster simulation, that we believe can exhibit approximatively the same final size distributions as (5) when $N \to \infty$. The concept revolves around employing a binned version of the state space (following the construction detailed in Section III A, with bin amplitude a) and defining a process that initiates particle nucleation in the first bin and subsequently grows them into adjacent bins with rates crafted to emulate the dynamics of (5), particularly focusing on the scenario of the diffusion kernel.

The i-th bin will then contain particles whose approximate size is ia and therefore a monomers will be needed to grow a particle to the next bin. Upon nucleation, particles immediately attain a size of a, necessitating once again a monomers for the reaction to proceed. Essentially, monomers will consistently be consumed in batches of a units. Hence, for simplicity, we can replace monomers with larger objects of size a, referred to as a-mers. It's worth noting that the size of an a-mer will increase with N, yet it will remain negligible compared to the typical size $\sqrt{N}$ of a particle. This approach ensures that both nucleation reactions and growth processes consume an a-mer. The initial number of a-mers will be $\lfloor \frac{N}{a} \rfloor$, increasing with N accordingly. Reactions will then be formulated in terms of chemical species D and B_i, representing a-mers and particles in the i-th bin, respectively. The corresponding chemical reaction network is

$$D \xrightarrow{\nu} B_1$$

$$B_i + D \xrightarrow{\gamma} B_{i+1} \qquad 1 \le i \le \lfloor \frac{N}{a} \rfloor - 1.$$

with state vector denoted by $\left(b_0, b_1, \ldots, b_{\lfloor \frac{N}{a} \rfloor} \right)$, and the (non mass-action) rate functions

The simulations of the approximated process are conducted using both the Gillespie and tau-leap methods whenever feasible (cf. Sections II B 1 and II B 2); the code is available at `https://github.com/elenasabbioni/nanoparticles`). It's readily apparent from Table I that significantly higher values of N can be explored with the approximated process due to reduced computational costs. The binned state space is considerably smaller than the original, and the number of growth reactions is also substantially diminished. Moreover, the computational advantage of the tau-leap algorithm is consistent, as the number of particles in each bin is larger and no longer causing failures of the post-leap checks.

In Figure 3, we present a comparison between the binned final size distributions obtained by

simulating the original process (5) with $N = 10^8$ (the maximum achievable magnitude), depicted using gray bars, alongside the size distribution obtained with the approximated process. To facilitate the comparison, for the approximated process, we replace the bars with lines that connect the heights of the bars.

The accuracy of the approximation at moderate N, particularly at $N = 10^8$, is somewhat lacking, especially in the right tail of the distribution. However, when scaling up to $N = 10^{12}$, the final size distribution of the approximated process starts to resemble the original one (although the right tail remains imperfect), and the variability is significantly reduced.

Comparing the final sizes obtained by the Gillespie algorithm with $N = 10^8$ and $N = 10^{12}$ reveals no distinguishable difference from those obtained using the tau-leap method. However, the tau-leap method allows us to scale N up to three orders of magnitude more, up to 10^{15}. Refer to Table I to observe the speed when the tau-leap method is used.

At $N = 10^{15}$, the final size density is nearly deterministic and perfectly aligns with that of the original process, accompanied by a remarkable reduction in noise.

D. Conclusions

We investigated the existence of a deterministic limit for the final particle size distribution of a stochastic model of nanoparticle growth under a scaling of the rate constants that was not previously addressed. By advanced simulation methods, we have observed the emergence of a deterministic limit for the particle size density as the initially available monomer units increase. However, the computational cost of these simulations imposes a constraint on the magnitude of monomer units that is significantly lower than realistic experimental conditions, hindering further investigation. To overcome this limitation, we developed a novel approximating process capable of significantly faster simulation while seemingly producing an equivalent limiting distribution. Leveraging this new approximation method, we succeeded in significantly increasing the magnitude of available monomer units, approaching levels expected in real experimental setups[27–29], thereby furnishing additional evidence of convergence toward a deterministic limit.

The findings presented in this paper set the stage for the mathematical proof of the existence of a deterministic limit for the final size distribution of nanoparticles and the analytical description of its density. Furthermore, there is potential interest in exploring the behavior of the stochastic model under alternate kernels beyond diffusion kernels.
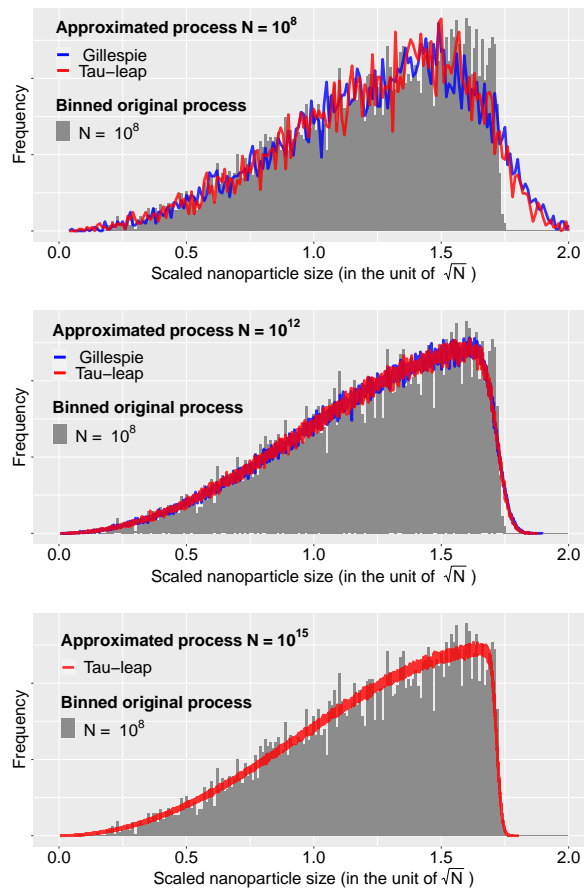
16

FIG. 3: Final size density of the original process (5) (gray bars), after that the state space has been binned, and final size density of the approximated process obtained with Gillespie (blue line) and with tau-leap algorithm (red line). The simulation for the original process is conducted with $N = 10^8$ in all three plots, while the approximated process is obtained with $N = 10^8$ (first row), $N = 10^{12}$ (second row) and $N = 10^{15}$ (third row). The last row exclusively presents results for the approximated process obtained through the tau-leap algorithm, due to limitations in scaling up to this magnitude using the Gillespie method. The reported particle sizes are scaled by $\sqrt{N}$. To enhance the comparison of histograms with different binnings and numbers of particles, the heights of the bars are scaled so that the area under each histogram is one.

The model we propose has further limitations: we do not consider reverse reactions, we neglect the coalescence of nanoparticles, and we do not consider spatial effects like diffusion, capture zones and large clusters interactions that are sometimes included in other models[42,43]. While most of these effects would complicate the model to a too large extent, the addition of reverse reactions, although not directly addressed in this paper, could be easily investigated using the

17

same methodology and would likely not significantly change the conclusions. Mathematically speaking, our model has many absorbing states: all those that are reached when all monomers are consumed. Reverse reactions would remove the absorption, since monomers could also be disaggregated from particles. This would make the model positive recurrent, and the concept of a *final* size distribution would not be meaningful and would need to be replaced by that of a *stationary* size distribution. When the purpose of the experiment is to create gold nanoparticles from monomers, reverse reactions are forced to occur with a negligible rate and the stationary size distribution would not differ significantly from our final one.

ACKNOWLEDGEMENTS

Appendix: Pseudocodes

We present here the pseudocodes of the algorithm outlined in Section II B, starting with the Gillespie's algorithm, described in Algorithm 1.

For what concerns the tau-leap with post-leap checks we introduce here the necessary notation. Let ST_k be the vector that stores the proposed internal times for reaction k, and SC_k the one storing the correspondent values of the Poisson process Y_k, i.e. $Y_k(ST_k) = SC_k$. Algorithm 2 shows the

18

Algorithm 1: Gillespie's algorithm

$X_0 \leftarrow N - n$, $X_n = 1$, $X_i \leftarrow 0$ for $i = 1, \cdots, N$ and $i \neq n$;

$L \leftarrow n$;   /* Dimension of the largest nanoparticle that has been created */

$\lambda_0 \leftarrow \nu N! / (N - n)!$, $\lambda_k \leftarrow 0$ for $k = 1, \cdots, N - 1$;   /* No growth at the beginning, */

$\pi := (\pi_0, \pi_1, \cdots, \pi_{N-1}) \leftarrow (1, 0, \cdots, 0)$;

while $X_0 > 0$ **do**

    Generate τ from Exponential with mean $\sum_{i=0}^{L} \lambda_i$;   /* It can be avoided in our case */

    for $k = 0, \cdots, L$ **do**

        $\pi_k \leftarrow \frac{\lambda_k}{\sum_{i=0}^{L} \lambda_i}$

    Generate r as a discrete random variable with values $0, 1, \cdots, N - 1$ and associated probabilities

    π;

    if $r = 1$ **then**

        $X_0 \leftarrow X_0 - n$;   /* Nucleation */

        $X_n \leftarrow X_n + 1$;

    else if $r = n, \cdots, L$ **then**

        $X_0 \leftarrow X_0 - 1$;   /* Growth */

        $X_r \leftarrow X_r - 1$;

        $X_{r+1} \leftarrow X_{r+1} + 1$;

        if $r = L$ **then**

            $L \leftarrow L + 1$;   /* Particles of dimension $L+1$ created */

    $\lambda_0 \leftarrow \nu X_0! / (X_0 - n)!$;   /* Update rates */

    $\lambda_k \leftarrow \gamma X_0 X_k$ for $k = 1, \cdots, L + 1$

---

initialization needed for the tau-leap with post leap checks, while Algorithm 3 presents the pseudo-code for all the following steps.

AUTHOR DECLARATIONS

Conflict of interest

The authors have no conflicts to disclose.

19

Algorithm 2: Initialization of tau-leap with post leap checks
---

$X_0 \leftarrow N - n$, $X_n = 1$, $X_i \leftarrow 0$ for $i = 1, \cdots, N$ and $i \neq n$;

$L \leftarrow n$;   `/* Dimension of the largest nanoparticle that has already been created, */`

$\lambda_0 \leftarrow \nu N!/(N-n)!$, $\lambda_k \leftarrow 0$ for $k = 1, \ldots, N-1,$;   `/* No growth at the beginning, */`

$T_k \leftarrow 0$, $C_k \leftarrow 0$ for $k = 0, \ldots, N-1$;

$ST_k \leftarrow 0$, $SC_k \leftarrow 0$;

$B_k \leftarrow 0$;   `/* Position of the greatest internal time explored in previous iterations */`

$row_k \leftarrow 0$;   `/* Position of the greatest internal time smaller than the one we are proposing */`

$g_0 \leftarrow g(X_0)$, $g_i \leftarrow 2$ for $i = 1, \ldots, N$;

$\mu_0 \leftarrow -n\lambda_0$, $\mu_n \leftarrow \lambda_0$, $\mu_i \leftarrow 0$ for $i \in \{1, \ldots, N\} \setminus \{n\}$;

$\sigma_0^2 \leftarrow n^2 \lambda_0$, $\sigma_n^2 \leftarrow \lambda_0$, $\sigma_i^2 \leftarrow 0$ for $i \in \{1, \ldots, N\} \setminus \{n\}$;

$\tau \leftarrow \min_{i \in [0,N]} \left(\frac{\max(\varepsilon X_i/g_i, 1)}{|\mu_i|}, \frac{\max(\varepsilon X_i/g_i, 1)^2}{\sigma_i^2} \right)$;

DATA AVAILABILITY STATEMENT

The data that supports the findings of this study are available within the article.

REFERENCES

[1] I. V. Zibareva, L. Y. Ilina, and A. A. Vedyagin, "Catalysis by nanoparticles: the main features and trends," Reaction Kinetics, Mechanisms and Catalysis **127**, 19–24 (2019).

[2] A. Saravanan, P. S. Kumar, S. Karishma, D.-V. N. Vo, S. Jeevanantham, P. Yaashikaa, and C. S. George, "A review on biosynthesis of metal nanoparticles and its environmental applications," Chemosphere **264**, 128580 (2021).

[3] G. Chen, I. Roy, C. Yang, and P. N. Prasad, "Nanochemistry and nanomedicine for nanoparticle-based diagnostics and therapy," Chemical Reviews **116**, 2826–2885 (2016).

[4] G. Martínez, M. Merinero, M. Pérez-Aranda, E. Pérez-Soriano, T. Ortiz, E. Villamor, B. Begines, and A. Alcudia, "Environmental impact of nanoparticles' application as an emerging technology: A review," Materials **14**, 166 (2020).

Algorithm 3: Tau-Leap with post-leap checks

Initialization as described in Algorithm 2;

while $X_0 > 0$ **do**

    for $k = 1:(L + 1)$ **do**

        $B_k \leftarrow \texttt{length}(ST_k)$;

        if $T_k + \lambda_k \tau \geq ST_k[B_k]$ **then**

            $J_k \leftarrow \text{Poisson}(T_k + \lambda_k \tau - ST_k[B_k]) + SC_k[B_k] - C_k$;   `/* Proposed internal time larger than all the`

            `previously proposed internal times */`

            $row_k \leftarrow B_k$

        else

            Find $2 \leq I_k \leq B_k - 1$ s.t. $ST_k[I_k - 1] \leq T_k + \lambda_k \tau \leq ST_k[I_k]$;

            $r \leftarrow \frac{T_k + \lambda_k \tau - ST_k[I_k - 1]}{ST_k[I_k] - ST_k[I_k - 1]}$;

            $J_k \leftarrow \text{Bin}(SC_k[I_k] - SC_k[I_k - 1], r) + SC_k[I_k - 1] - C_k$;   `/* Proposed internal time between two previously`

            `proposed times */`

            $row_k \leftarrow I_k - 1$;

    if *leap-condition* (8) *holds* **then**

        for $k = 1, \ldots, L$ **do**

            Move all the rows of ST_k and SC_k greater than $row_k + 1$ up to positions 2, set first rows equal to $T_k + \lambda_k$ and $C_k + J_k$

            respectively;

            $T_k \leftarrow T_k + \lambda_k \tau$ and $C_k \leftarrow C_k + J_k$;

        $t \leftarrow t + \tau$;   `/* Update absolute time */`

        if *leap condition* (8) *holds also with* $\frac{3}{4}\varepsilon$ **then**

            $\tau \leftarrow \tau^q$;

        else

            $\tau \leftarrow \tau p^*$;

        $X_0 \leftarrow X_0 - nJ_0 - \sum_{k=1}^{L} J_k$;   `/* Update states */`

        $X_n \leftarrow X_n - J_n + J_0$;

        for $i = n + 1, \ldots, L$ **do**

            $X_i \leftarrow X_i - J_i + J_{i-1}$

        $X_{L+1} \leftarrow X_{L+1} + J_L$;

        $\lambda_0 \leftarrow \nu X_0!/(X_0 - n)!$;   `/* Update rates */`

        $\lambda_k \leftarrow \gamma X_0 X_k$ for $k = 1, \ldots, L+1$;

        if$J_L > 0$ **then** $L \leftarrow L + 1$

    else

        for $k = 1, \ldots, L$ **do**

            Add new rows $[T_k + \lambda_k \tau]$ and $[C_k + J_k]$ between rows row_k and $row_k + 1$ of ST_k and SC_k respectively

        $\tau \leftarrow \tau p$

---

[5]R. Ettlinger, U. Lächelt, R. Gref, P. Horcajada, T. Lammers, C. Serre, P. Couvreur, R. E. Morris, and S. Wuttke, "Toxicity of metal–organic framework nanoparticles: from essential analyses to potential applications," Chemical Society Reviews **51**, 464–484 (2022).

[6]V. E. Katzourakis and C. V. Chrysikopoulos, "Modeling the transport of aggregating nanoparticles in porous media," Water Re-

21

sources   Research   **57**   (2021),   https://doi.org/10.1029/2020WR027946, https://agupubs.onlinelibrary.wiley.com/doi/pdf/10.1029/2020WR027946.

[7] B. Szała-Mendyk, A. Drajkowska, and A. Molski, "Modified smoluchowski rate equations for aggregation and fragmentation in finite systems," The Journal of Physical Chemistry B **127**, 6154–6162 (2023), https://doi.org/10.1021/acs.jpcb.3c02884.

[8] V. K. LaMer and R. H. Dinegar, "Theory, production and mechanism of formation of monodispersed hydrosols," Journal of the American Chemical Society **72**, 4847–4854 (1950).

[9] V. K. LaMer, "Nucleation in phase transitions," Industrial & Engineering Chemistry **44**, 1270–1277 (1952).

[10] J. Farjas and P. Roura, "Modification of the kolmogorov–johnson–mehl–avrami rate equation for non-isothermal experiments and its analytical solution," Acta Materialia **54**, 5573–5579 (2006).

[11] D. Hömberg, F. S. Patacchini, K. Sakamoto, and J. Zimmer, "A revisited johnson–mehl–avrami–kolmogorov model and the evolution of grain-size distributions in steel," IMA Journal of Applied Mathematics **82**, 763–780 (2017).

[12] M. Fanfoni and M. Tomellini, "The johnson-mehl- avrami-kohnogorov model: A brief review," Il Nuovo Cimento D **20**, 1171–1182 (1998).

[13] M. A. Watzky and R. G. Finke, "Transition metal nanocluster formation kinetic and mechanistic studies. a new mechanism when hydrogen is the reductant: Slow, continuous nucleation and fast autocatalytic surface growth," Journal of the American Chemical Society **119**, 10382–10400 (1997).

[14] M. A. Watzky, E. E. Finney, and R. G. Finke, "Transition-metal nanocluster size vs formation time and the catalytically effective nucleus number: A mechanism-based treatment," Journal of the American Chemical Society **130**, 11959–11969 (2008).

[15] D. R. Handwerk, P. D. Shipman, C. B. Whitehead, S. Özkar, and R. G. Finke, "Mechanism-enabled population balance modeling of particle formation en route to particle average size and size distribution understanding and control," Journal of the American Chemical Society **141**, 15827–15839 (2019).

[16] M. A. Watzky and R. G. Finke, "Pseudoelementary steps: A key concept and tool for studying the kinetics and mechanisms of complex chemical systems," The Journal of Physical Chemistry A **125**, 10687–10705 (2021).

[17] O. Penrose, "Metastable states for the becker-döring cluster equations," Communications in Mathematical Physics **124**, 515–541 (1989).

22

[18] M. Slemrod, "The becker-döring equations," in *Modeling in Applied Sciences: A Kinetic Theory Approach* (Springer, 2000) pp. 149–171.

[19] E. Hingant and R. Yvinec, "Deterministic and stochastic becker–döring equations: Past and recent mathematical developments," in *Stochastic Processes, Multiscale Modeling, and Numerical Methods for Computational Cellular Biology* (Springer International Publishing, 2017) pp. 175–204.

[20] P. Laurençot and S. Mischler, "From the becker–döring to the lifshitz–slyozov–wagner equations," Journal of Statistical Physics **106**, 957–991 (2002).

[21] A. Damialis, "The lifshitz–slyozov–wagner equation for reaction-controlled kinetics," Proceedings of the Royal Society of Edinburgh: Section A Mathematics **140**, 273–289 (2010).

[22] I. Jeon, "Existence of gelling solutions for coagulation-fragmentation equations," Communications in Mathematical Physics **194**, 541–567 (1998).

[23] R. Szabó and G. Lente, "Full analytical solution of a nucleation-growth type kinetic model of nanoparticle formation," Journal of Mathematical Chemistry **57**, 616–631 (2018).

[24] R. Szabó and G. Lente, "General nucleation-growth type kinetic models of nanoparticle formation: possibilities of finding analytical solutions," Journal of Mathematical Chemistry **59**, 1808–1821 (2021).

[25] R. Szabó and G. Lente, "A comparison of the stochastic and deterministic approaches in a nucleation–growth type model of nanoparticle formation," Chemistry of Materials **33**, 5430–5436 (2021).

[26] R. Szabó and G. Lente, "Deterministic approximation for the nucleation-growth type model of nanoparticle formation: A validation against stochastic simulations," Chemical Engineering Journal **446**, 137377 (2022).

[27] A. Forgács, K. Moldován, P. Herman, E. Baranyai, I. Fábián, G. Lente, and J. Kalmár, "Kinetic model for hydrolytic nucleation and growth of TiO_2 nanoparticles," The Journal of Physical Chemistry C **122**, 19161–19170 (2018).

[28] B. Peter, I. Lagzi, S. Teraji, H. Nakanishi, L. Cervenak, D. Zámbó, A. Deák, K. Molnár, M. Truszka, I. Szekacs, and R. Horvath, "Interaction of positively charged gold nanoparticles with cancer cells monitored by an in situ label-free optical biosensor and transmission electron microscopy," ACS Applied Materials Interfaces **10**, 26841–26850 (2018).

[29] S. Labidi, Z. Jia, M. B. Amar, K. Chhor, and A. Kanaev, "Nucleation and growth kinetics of zirconium-oxo-alkoxy nanoparticles," Physical Chemistry Chemical Physics **17**, 2651–2659

23

(2015).

[30] A. G. Shard, L. Wright, and C. Minelli, "Robust and accurate measurements of gold nanoparticle concentrations using UV-visible spectrophotometry," Biointerphases **13**, 061002 (2018), https://pubs.aip.org/avs/bip/article-pdf/doi/10.1116/1.5054780/19743906/061002_1_online.pdf.

[31] D. T. Gillespie, A. Hellander, and L. R. Petzold, "Perspective: Stochastic algorithms for chemical kinetics," The Journal of Chemical Physics **138**, 170901 (2013).

[32] D. F. Anderson, "Incorporating postleap checks in tau-leaping," The Journal of Chemical Physics **128** (2008), 10.1063/1.2819665.

[33] J. Bezanson, A. Edelman, S. Karpinski, and V. B. Shah, "Julia: A fresh approach to numerical computing," SIAM review **59**, 65–98 (2017).

[34] D. F. Anderson and T. G. Kurtz, *Stochastic analysis of biochemical systems*, Vol. 674 (Springer, 2015).

[35] S. N. E. Thomas G. Kurtz, *Markov Processes: Characterization and Convergence* (John Wiley and Sons, Inc, 1986).

[36] A. Vasseur, F. Poupaud, J.-F. Collet, and T. Goudon, "The beker–döring system and its lifshitz–slyozov limit," SIAM Journal on Applied Mathematics **62**, 1488–1500 (2002).

[37] J. Deschamps, E. Hingant, and R. Yvinec, "Quasi steady state approximation of the small clusters in becker–döring equations leads to boundary conditions in the lifshitz–slyozov limit," Communications in Mathematical Sciences **15**, 1353 – 1384 (2017).

[38] D. T. Gillespie, "A general method for numerically simulating the stochastic time evolution of coupled chemical reactions," Journal of Computational Physics **22**, 403–434 (1976).

[39] D. T. Gillespie, "Exact stochastic simulation of coupled chemical reactions," The Journal of Physical Chemistry **81**, 2340–2361 (1977).

[40] P. Érdi and G. Lente, *Stochastic Chemical Kinetics* (Springer New York, 2014).

[41] D. T. Gillespie, "Approximate accelerated stochastic simulation of chemically reacting systems," The Journal of chemical physics **115**, 1716–1733 (2001).

[42] D. Kandel, "Selection of the scaling solution in a cluster coalescence model," Phys. Rev. Lett. **79**, 4238–4241 (1997).

[43] D. J. Aldous, "Deterministic and stochastic models for coalescence (aggregation and coagulation): A review of the mean-field theory for probabilists," Bernoulli **5**, 3–48 (1999).